Journal of Materials Chemistry C

PAPER

View Article Online
View Journal | View Issue

Cite this: J. Mater. Chem. C, 2016, 4, 8416

A surface oxide thin layer of copper nanowires enhanced the UV selective response of a ZnO film photodetector†

Feng Teng, Lingxia Zheng, Kai Hu, Hongyu Chen, Yanmei Li, Zhiming Zhang and Xiaosheng Fang*

Received 10th July 2016,
Accepted 16th August 2016

DOI: 10.1039/c6tc02901a

www.rsc.org/MaterialsC

Copper nanowires (Cu NWs) with good crystallinity and high aspect ratio were prepared by a facile hydrothermal method at low temperature, and they were dispersed on a smooth and thin layer of ZnO film to construct a photodetector (PD). This Cu NW/ZnO PD exhibits a remarkably higher UV-visible rejection ratio (~160), which is almost 13 times that of a bare ZnO PD (12.5) and more than twice that of a Cu film/ZnO PD (67.7). The high UV light selective response of the Cu NW/ZnO PD is caused by the dramatic decrease of the photoresponsivity in the visible light region and the high photocurrent in the UV region due to the presence of a potential barrier between ZnO and Cu NWs. Interestingly, the commonly observed thin layer of CuO (2 nm) on the surface of Cu NWs plays a significant role in the enhanced UV light selective response performance. The results demonstrate that the height of the Schottky barrier and the thickness of the depletion layer are both reduced owing to the oxidized copper layer, which leads to the excellent UV selective response. Our results indicate that Cu NWs, as a multifunctional material, could have diverse applications in the field of optoelectronics. And this detector obtained by a simple preparation method shows great potential in the actual applications in the future.

1. Introduction

Photodetectors (PDs), especially ultraviolet (UV) PDs, have received much attention in recent years because of their great value and potential application in the field of military, safety warning, optical communication and industrial production.[1–8] Among the common materials, ZnO has been regarded as one of the most promising candidates for UV PDs because of its high carrier mobility and wide band gap (~3.37 eV).[9–11] Due to their virtues of structural simplicity, low-cost fabrication and large scale preparation, ZnO film-based UV PDs exhibit great potential in practical applications.[12,13] The reported ZnO films are all polycrystalline, which could generate photoresponse under both UV light and visible light illumination due to the existence of a large number of surface defects on ZnO nanograins. Meanwhile, the slow O_2 adsorption/desorption processes on the ZnO film lead to the long rise/decay time of bare ZnO film PDs.[14,15]

In order to improve the performance of ZnO film based PDs, surface modified ZnO nanostructures (*e.g.* capped by PVA,[16] ZnS,[17] Au nanoparticles[15] and carbon nanomaterials[18,19]), ZnO based Schottky junction,[20] p–n junction[21] and heterojunction structures have been prepared and demonstrated excellent optoelectronic performance due to the decrease of adsorbed O_2 or the addition of a potential barrier.

Recently, copper nanomaterials, especially copper nanowires (Cu NWs), have shown unique advantages in the field of optoelectronics, electronics, transparent conductive electrodes (TCEs) and flexible electrodes due to their excellent conductivity, large specific surface area and abundant availability.[22–25] In particular, Cu NWs prepared by a facile hydrothermal method at low temperature have been widely studied due to their high electric conductivity, high thermal conductivity and ease of fabrication, and are used as the active material of heat dissipation,[26,27] as the electrode material of photovoltaic devices[28,29] and as the matrix material of water splitting.[30] And it is commonly known that the thin Cu NWs are intrinsically unstable under ambient conditions and are easily oxidized, which is harmful to the application of TCEs.[31,32] Nevertheless, the oxide layer on the surface of Cu NWs still has some advantages under certain conditions because copper oxides are good p-type semiconductors.

Herein, Cu NWs obtained by a simple hydrothermal method with good crystallinity and high aspect ratio were dropped on a

Department of Materials Science, Fudan University, Shanghai, 200433, P. R. China. E-mail: xshfang@fudan.edu.cn

† Electronic supplementary information (ESI) available: The cross-sectional image of spin-coated ZnO film, the XPS spectrum of Cu 2p, semi-log *I–V* curves of a Cu NW/ZnO PD in the dark and under 500, 400 and 360 nm light illumination, the normalized photoresponsivity spectra of the Cu NW/ZnO PD with the light illuminated from the back side, and their data comparison with other similar structures. See DOI: 10.1039/c6tc02901a

ZnO film to form Cu NW/ZnO composites, which demonstrated excellent UV light selective response properties. Compared with the original Schottky junction formed at the interface between Cu film and ZnO, the thin oxide layer that existed on the surface of Cu NWs exerts an influence on the height of the Schottky barrier, which results in smaller photocurrent under visible light illumination and larger photocurrent in the UV light region, thus leading to a higher UV-visible rejection ratio. Though the light absorption and scattering of Cu NWs also affect the photocurrent in the visible light region, this is not the main reason for the high UV selective response properties. These results demonstrate the potential of Cu NWs in optoelectronic applications and also provide experimental data support for the further development of ZnO film based PDs in future practical applications.

2. Experimental

Synthesis of copper nanowires

Cu NWs were synthesized by a green hydrothermal method according to a previous report with slight modification.[33] Typically, 200 mg of $CuCl_2{\cdot}2H_2O$, 300 mg of glucose and 1.17 g of hexadecylamine (HDA) were sufficiently stirred in 80 ml of deionized water at room temperature for 16 h, and then transferred to a 100 ml Teflon-lined autoclave to react at 100 °C for 24 h. The product was collected and washed by water, ethanol and hexane, respectively. The as-prepared Cu NWs were dispersed in hexane to produce Cu ink (10 mg ml^{-1}), which could retard the oxidation process of Cu NWs.

Device fabrication

The ZnO precursor was constituted by 1.44 g of $Zn(CH_3COO)_2{\cdot}2H_2O$, 0.75 g of poly(vinyl alcohol) (PVA-1788 low-viscosity, $M_w \sim 44.05$), 10 ml of water and 0.5 ml of CH_3COOH.[34] The ZnO film was prepared by spin-coating the precursor solution on a glass substrate for three times at 3000 rpm for 20 s, and then annealed in air at 450 °C for 2 h. The thickness of as-obtained ZnO film was about 100 nm, as shown in Fig. S1 (ESI†). For the preparation of Cu NW/ZnO composites, one drop of Cu ink was dropped on the ZnO film, and then two pieces of Ag paste were covered on the Cu NWs and ZnO film, respectively. For comparison, a Cu film (100 nm) was prepared on the ZnO film by the e-beam evaporation method and assembled as a Cu film/ZnO PD using the same method.

Characterization

The morphology of Cu NWs and ZnO film was characterized by field-emission scanning electron microscopy (FESEM, Zeiss sigma) and high resolution transmission electron microscopy (HRTEM, TECNAL G^2 S-TWIN). X-ray diffraction patterns were collected on a Bruker D8-A25 diffractometer equipped with Cu Kα radiation ($\lambda = 1.5405$ Å). The surface chemical environment of Cu NWs was measured using a PHI 5000C EASA system X-ray photoelectron spectroscopy (XPS), with a C1s peak at 284 eV as the standard signal. The optical absorption spectra were investigated using a UV-vis spectrophotometer (Hitachi U-3900H).

Optoelectronic measurements

The optoelectronic properties (I–V, I–t) were characterized using a semiconductor characterization system (Keithley 4200-SCS) equipped with a 75 W xenon arc lamp light source and a standard synchronous detection scheme. The photoresponsivity spectra of the samples were obtained by collecting the current value at 1 V bias under different wavelengths of light illumination. All the measurements were carried out under ambient conditions.

3. Results and discussion

Cu NWs were synthesized by the hydrothermal method at low temperature through the chemical reaction of copper chloride in an aqueous solvent in the presence of glucose and hexadecylamine (HDA), according to a previous study.[33] The HDA used here not only acts as the capping agent to restrict the growth direction of Cu NWs, but it also participates in the reduction reaction of Cu^{2+} ions combined with glucose.[35] Fig. 1a and b show the structural morphology of the obtained Cu NWs. From the low-resolution scanning electron microscopy (SEM) image, it can be observed that the length of the Cu NWs can reach several micrometres. Fig. 1b shows that the Cu NWs exhibit a smooth surface with very few impurities (*e.g.* nanoparticles) and the diameters are approximately 50–150 nm. The aspect ratio is as high as 10^2 to 10^3, which is greatly valuable in the application of TCEs. Fig. 1c and d show that the ZnO film prepared by the spin-coating method has good uniformity. It consists of a large amount of nanograins with their sizes ranging from several nanometres to hundreds of nanometres. For Cu NW/ZnO composites, the Cu NWs are well distributed on the top of the ZnO film and leave part of the ZnO exposed to the environment (Fig. 1e and f), which is highly favourable for light harvesting.

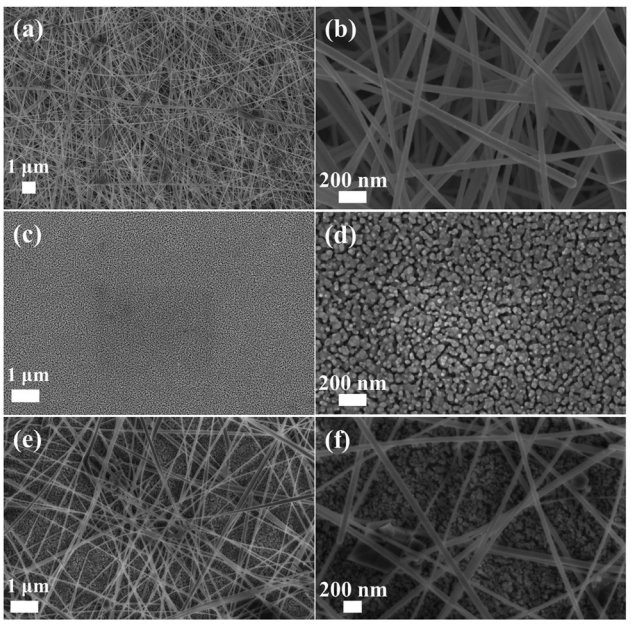

Fig. 1 The low resolution SEM images of (a) the Cu NWs, (c) ZnO film and (e) Cu NW/ZnO composite. And (b), (d) and (f) are the corresponding high resolution SEM images.

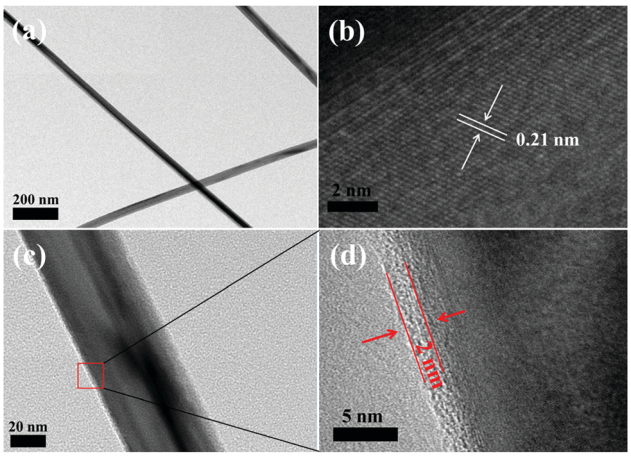

Fig. 2 (a and c) The TEM images and (b and d) HR-TEM images of the obtained Cu NWs.

To further examine the morphology of Cu NWs, high-resolution transmission electron microscopy (HRTEM) was performed and the results are shown in Fig. 2. The Cu NWs are straight with diameters of ~50–100 nm, and their extraordinary length is of tens of micrometers, which is consistent with the SEM images in Fig. 1a. The HRTEM image in Fig. 2b confirms the high crystallinity with a lattice fringe distance of 0.21 nm, consistent with the Cu{111} interplanar spacing. There is a very thin oxide layer (~2 nm, as shown in Fig. 2d) on the surface of Cu NWs, which may be caused by the oxidation process in air. And the morphology of Cu NWs remains the same even after one month of exposure to air, demonstrating that they have high stability, which is different to that obtained by the reduction of hydrazine hydrate ($N_2H_4{\cdot}H_2O$).[36]

Fig. 3a shows the X-ray diffraction (XRD) patterns of Cu NWs and ZnO film. For the ZnO film, the peaks located at 34.43, 36.3 and 63.1° correspond to the {002}, {101} and {103} planes of the ZnO crystalline films (JCPDS #36-1451), respectively. And for Cu NWs,

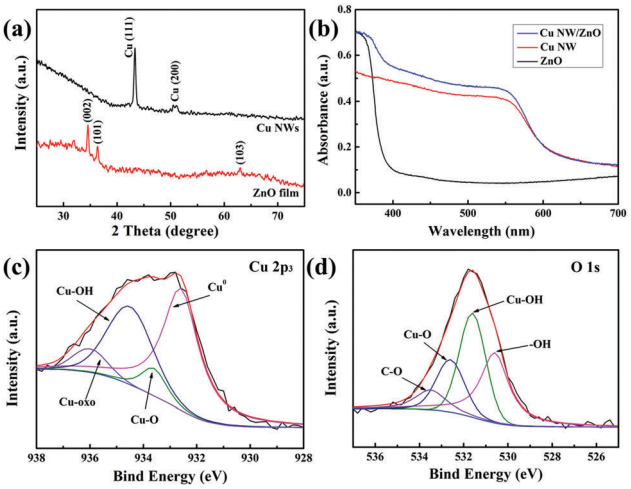

Fig. 3 (a) The XRD patterns of the Cu NWs and ZnO film, (b) absorption spectra of the Cu NWs, ZnO film and Cu NW/ZnO composite. The fitting XPS spectra of (c) Cu $2p_3$ and (d) O 1s.

the peaks at 43.3° and 50.5° correspond to the {111} and {200} planes of the fcc copper (JCPDS #03-1018), respectively, which is consistent with the TEM images and the previous literature studies.[23,37] The UV-vis absorption spectra of Cu NWs, ZnO film and Cu NW/ZnO composites are shown in Fig. 3b. The ZnO film has very weak light absorption in the visible region, but its light absorption in the UV region (300–400 nm) is very strong. The Cu NWs exhibit obvious light absorption in the range of 350–560 nm, which also has a certain relationship with the surface plasmon resonance effect and the light scattering phenomenon of the Cu NWs.[23] After Cu NWs were covered on the ZnO film, the composite exhibits a similar spectral profile to that of Cu NWs, with enhanced light absorbance in the UV region caused by ZnO film, which demonstrates that the Cu NWs could not shelter the ZnO film thoroughly.

To examine the chemical states of the Cu NWs, X-ray photoelectron spectral (XPS) analysis was performed. The characteristic binding energy values can directly identify elements that exist in or on the surface of the material being analyzed. Fig. S2 (ESI†) displays the XPS spectrum of Cu 2p. Obviously, the signals of Cu $2p_{3/2}$ (930–938 eV) and Cu $2p_{1/2}$ (around 955 eV) can be observed, and the satellite peaks that appear at 940–945 eV and 960–965 eV demonstrate the existence of CuO on the surface of the Cu NWs, in good agreement with TEM results in Fig. 2d.[35] To obtain in-depth and comprehensive information about the surface composition of Cu NWs, the oxidation states of copper on the surface are studied in detail by XPS peak differentiation imitating analysis. Fig. 3c and d show the deconvolution of XPS spectra in the Cu $2p_{3/2}$ and O 1s regions. Two main peaks observed at 932.6 eV and 934.5 eV are assigned to the Cu element and $Cu(OH)_2$, respectively, and two small peaks (933.6 and 936 eV)[38] are attributed to CuO and mono-(mu-oxo) dicopper,[39] respectively. The corresponding O 1s spectra of the sample (Fig. 3d) display three main peaks at 530.6, 531.6 and 532.6 eV for hydroxyl, Cu–OH and Cu–O bonds, respectively, which further confirms the existence of CuO and $Cu(OH)_2$. The weak peak that appeared at 533.5 eV for the C–O bond might originate from the adsorbed organics.

The photoelectric properties of ZnO film and Cu NW/ZnO composites were carefully examined by constructing them into PDs with two pieces of silver paste as the electrodes, as shown in the schematic diagram (Fig. 4a). As the Cu NW/ZnO composite exhibits obvious light absorption over the region of 350–560 nm (Fig. 3b), we measured the current–voltage (*I–V*) curves of the Cu NW/ZnO PD in the dark and under light illumination of 360, 400 and 500 nm when the bias was swept from −1 V to +1 V. As shown in Fig. S3 (ESI†), the photocurrent dramatically increases under the UV light (360 nm) illumination while only a small photocurrent increase is observed under the visible light illumination (400 and 500 nm). In order to clarify the role of the Schottky barrier in the optoelectronic performance of Cu/ZnO composites, a Cu film/ZnO PD was also prepared by evaporation of Cu film on the ZnO film. For a UV photodetector, the UV-visible rejection ratio is an important parameter, which reflects the ability of a detector to detect the UV light from a messy light source. The higher the UV-visible rejection ratio,

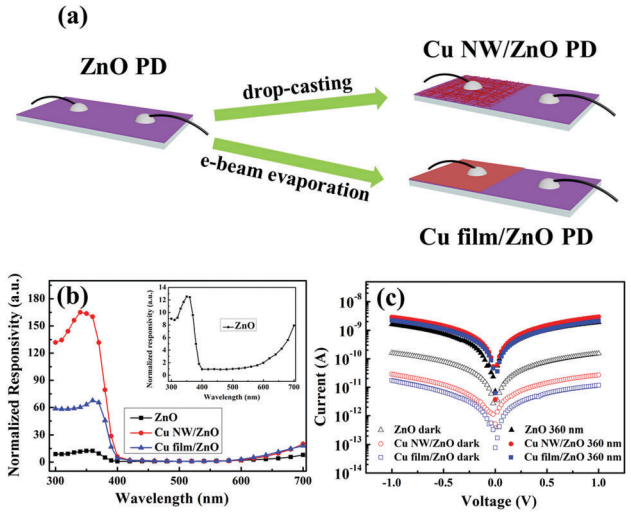

Fig. 4 (a) Schematic illustration of the fabricated PDs based on ZnO film, Cu NW/ZnO composite and Cu film/ZnO composite. (b) The normalized responsivity spectra of the ZnO PD, the Cu film/ZnO PD and the Cu NW/ZnO PD; the inset shows the normalized responsivity of the bare ZnO PD. (c) The semilog *I*–*V* curves of the three obtained PDs in the dark and under 360 nm illumination.

the greater its potential in practical applications. The UV-visible rejection ratio (normalized responsivity) is defined as:

$$\text{Normalized responsivity} = R(\lambda)/R(500\ \text{nm})$$

where $R(\lambda)$ is the photoresponsivity of detector under the light illumination at λ nm. Fig. 4b displays the normalized photoresponsivity spectra of the bare ZnO film PD, the Cu NW/ZnO PD and the Cu film/ZnO PD when the applied bias was 1 V. It can be observed that the normalized responsivity remains the same in the visible region for all three PDs, except that the photoresponsivity appeared from 600 to 700 nm, which may be caused by the two photon excitation effect and surface defects of the ZnO polycrystalline film.[40] From the inset of Fig. 4b, it can be seen that the maximum normalized responsivity of the bare ZnO film PD in the UV region is only 12.52 at 350 nm, and the value at 700 nm can reach 7.9, which would lead to incorrect results in practical applications. For the Cu NW/ZnO PD, the maximum normalized responsivity in the UV region can reach 160, which is an order of magnitude higher than that of the bare ZnO film PD, demonstrating its good UV detective performance compared with other similar structures (as shown in Table S1, ESI†). And the value at 700 nm is only 20.2, which is much smaller than that in the UV region. These results demonstrate that the Cu NW/ZnO PD shows significantly different photoresponse performance between UV and visible light, indicating the high UV light selective response characteristics. For the Cu film/ZnO PD, the maximum normalized responsivity in the UV region is 67.7 at 360 nm, 5 times that of the ZnO PD, meaning its obvious UV light selective response, but smaller than that of the Cu NW/ZnO PD. The high UV light selective response properties of the Cu NW/ZnO PD should be attributed to the dramatic decrease of the responsivity in the visible light region (3.9 μA W^{-1} under 500 nm illumination), which is much smaller than that of the Cu film/ZnO PD (16 μA W^{-1}) and the ZnO PD (78 μA W^{-1}), caused by the potential barrier between Cu NWs and ZnO. Fig. 4c shows the *I*–*V* characteristics of the aforementioned three PDs in the dark and under UV illumination (360 nm). The dark currents for the Cu film/ZnO PD and the Cu NW/ZnO PD are much smaller than that of the bare ZnO PD, which is caused by the Schottky barrier formed at the interface of copper and ZnO. Due to the existence of a CuO thin layer on the surface of Cu NWs, the height of the Schottky barrier reduces slightly, which leads to larger dark current compared with the Cu film/ZnO PD. The photocurrents of the Cu NW/ZnO PD and the Cu film/ZnO PD are basically the same as the bare ZnO PD under 360 nm illumination, except a little difference under negative bias, which may still be caused by the Schottky barrier.

Fig. 5a presents the light on/off switching characteristics (at a bias of 1 V) of the three PDs under 360 nm UV light illumination (with an intensity of 0.8 mW cm^{-2}). All the PDs exhibit highly stable photoresponse upon repeatedly switching the light on/off. The photocurrent follows the order: Cu NW/ZnO PD > Cu film/ZnO PD > bare ZnO PD. From the normalized *I*–*t* curve of all PDs (Fig. 5b), the rise times of the Cu film/ZnO PD and the Cu NW/ZnO PD are about 7.59 and 10.35 s, respectively, much shorter than that of the bare ZnO film PD (12.48 s), resulting from the high electron

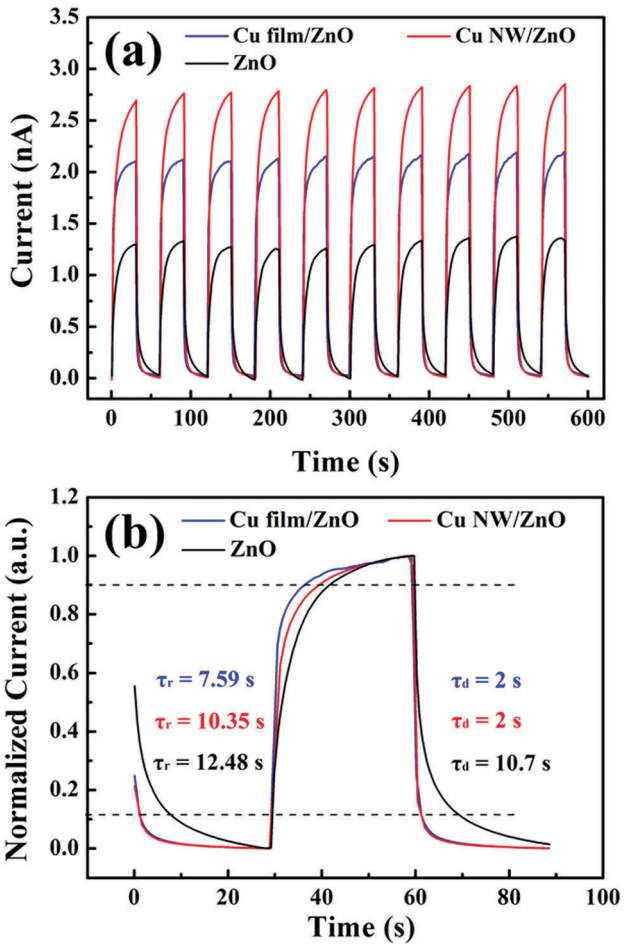

Fig. 5 (a) *I*–*t* curves of the three PDs at +1 V bias under 360 nm illumination. (b) The normalized *I*–*t* curves of the obtained PDs.

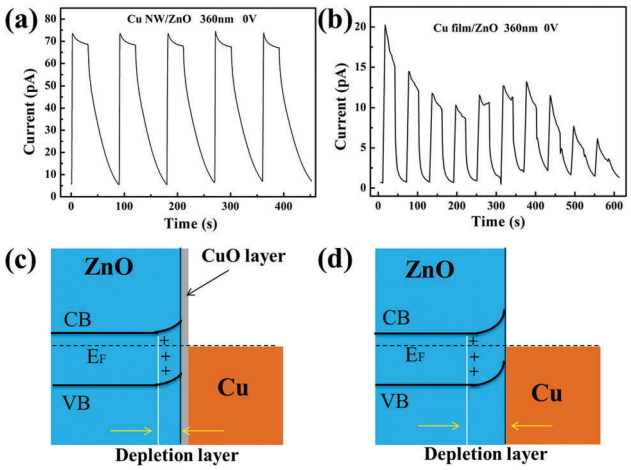

Fig. 6 The *I*–*t* curves at zero bias under 360 nm illumination for (a) Cu NW/ZnO PD and (b) Cu film/ZnO PD. (c and d) Schematic illustration of the energy levels of the Cu NW/ZnO PD and the Cu film/ZnO PD, respectively.

transport efficiency of Cu film and Cu NWs (the rise time is defined as the time for the current to rise from 10% to 90% of the peak value). The decay times of the Cu film/ZnO PD (~2 s) and the Cu NW/ZnO PD (~2 s) are also much shorter than that of the bare ZnO film PD (~10.7 s), which should be attributed to the presence of a Schottky barrier between copper and ZnO (the decay time is defined as the time for the current to decay from 90% to 10% of the peak value).

In order to further evaluate the photodetection performance influenced by the existence of a CuO layer, we tested the time-dependent current curves of the Cu NW/ZnO PD and the Cu film/ZnO PD at zero bias under 360 nm UV illumination. From Fig. 6a and b, it can be observed that the Cu NW/ZnO PD shows a stable photocurrent response (~70 pA) at zero bias while the photocurrent of the Cu film/ZnO PD is weaker and unstable, which implies that the CuO layer plays an important role in the high UV selective response properties of the Cu NW/ZnO PD. Fig. 6c and d display the schematic illustration of the energy levels of the Cu NW/ZnO PD and the Cu film/ZnO PD. Due to the presence of a CuO layer acting as a transition layer between ZnO and Cu, the height of the Schottky barrier and the thickness of the depletion layer are both reduced, which leads to high photocurrent in the UV region. Considering that the Cu NWs can absorb and scatter the visible light to a certain extent, the photoresponsivity spectrum of the Cu NW/ZnO PD illuminated from the back side is obtained (Fig. S4, ESI†). It shows a similar spectral profile with relatively lower values, indicating that the light absorption and scattering effect of Cu NWs is not the major reason for the decrease of photocurrent in the visible light region, which further confirms that the potential barrier formed at the interface of Cu NW/ZnO is the main reason for the enhancement of UV light selective response characteristics.

4. Conclusions

In summary, Cu NW/ZnO composite was fabricated by dispersing the Cu NWs synthesized by a simple hydrothermal method at low temperature on the spin coated ZnO film and constructed into a photodetector. The obtained Cu NW/ZnO PD exhibits an excellent UV light selective response with a UV-visible rejection ratio of 167, which is one order of magnitude higher than that of the bare ZnO film PD (12.5), showing its great potential in future practical applications. The high UV light selective response is caused by the warped Schottky barrier formed at the interface of Cu NWs and ZnO. Furthermore, the Cu NW/ZnO PD has an obvious and stable photocurrent (~70 pA) under 360 nm UV light illumination at zero bias, demonstrating that the CuO layer on the surface of Cu NWs can reduce the height of Schottky barrier formed between ZnO and copper. The light absorption and scattering effect of Cu NWs also affect its photoresponsivity in visible light region, but it is not the major reason for the high UV light selective response characteristics of Cu NW/ZnO PD. The high performance UV detector prepared by such a simple method would exhibit its great potential in future practical applications.

Acknowledgements

This work was supported by the National Natural Science Foundation of China (Grant No. 51471051), National Postdoctoral Science Foundation of China (2016M591603), Science and Technology Commission of Shanghai Municipality (15520720700), Shanghai Shu Guang Project (12SG01), and the Programs for Professor of Special Appointment (Eastern Scholar) at Shanghai Institutions of Higher Learning.

References

1 X. Li, C. Gao, H. Duan, B. Lu, Y. Wang, L. Chen, Z. Zhang, X. Pan and E. Xie, *Small*, 2013, **9**, 2005–2011.
2 Z. Yang, M. Q. Wang, X. H. Song, G. D. Yan, Y. C. Ding and J. B. Bai, *J. Mater. Chem. C*, 2014, **2**, 4312–4319.
3 H. N. Cong, G. D. Wei, H. L. Hou, H. J. Yang, M. H. Shang, F. M. Gao, W. Y. Yang and G. Z. Shen, *Nano Res.*, 2015, **8**, 2822–2832.
4 L. Peng, L. F. Hu and X. S. Fang, *Adv. Funct. Mater.*, 2014, **24**, 2591–2610.
5 L. Gan, M. Y. Liao, H. Q. Li, Y. Ma and T. Y. Zhai, *J. Mater. Chem. C*, 2015, **3**, 8300–8306.
6 H. Y. Chen, H. Liu, Z. M. Zhang and X. S. Fang, *Adv. Mater.*, 2016, **28**, 403–433.
7 D. S. Zheng, J. L. Wang, W. D. Hu, L. Liao, H. H. Fang, N. Guo, P. Wang, F. Gong, X. D. Wang, Z. Y. Fan, X. Wu, X. J. Meng, X. S. Chen and W. Lu, *Nano Lett.*, 2016, **16**, 2548–2555.
8 Z. He, Q. Liu, H. Hou, F. Gao, B. Tang and W. Y. Yang, *ACS Appl. Mater. Interfaces*, 2015, **7**, 10878–10885.
9 H. Y. Chen, K. W. Liu, L. F. Hu, A. A. Al-Ghamdi and X. S. Fang, *Mater. Today*, 2015, **18**, 493–502.
10 S. Liu, Q. Liao, S. Lu, Z. Zhang, G. Zhang and Y. Zhang, *Adv. Funct. Mater.*, 2016, **26**, 1347–1353.
11 G. Shoute, A. Afshar, T. Muneshwar, K. Cadien and D. Barlage, *Nat. Commun.*, 2016, **7**, 10632.

12 C. Tian, D. Jiang, B. Li, J. Lin, Y. Zhao, W. Yuan, J. Zhao, Q. Liang, S. Gao, J. Hou and J. Qin, *ACS Appl. Mater. Interfaces*, 2014, **6**, 2162–2166.
13 Z. Zou, C. Xie, S. Zhang, C. Yang, G. Zhang and L. Yang, *Sens. Actuators, B*, 2013, **188**, 1158–1166.
14 Z. Jin, Q. Zhou, Y. Chen, P. Mao, H. Li, H. Liu, J. Wang and Y. Li, *Adv. Mater.*, 2016, **28**, 3697–3702.
15 K. Liu, M. Sakurai, M. Liao and M. Aono, *J. Phys. Chem. C*, 2010, **114**, 19835–19839.
16 A. Bera and D. Basak, *ACS Appl. Mater. Interfaces*, 2009, **1**, 2066–2070.
17 A. Bera and D. Basak, *ACS Appl. Mater. Interfaces*, 2010, **2**, 408–412.
18 H. Liu, Q. Sun, J. Xing, Z. Zheng, Z. Zhang, Z. Lu and K. Zhao, *ACS Appl. Mater. Interfaces*, 2015, **7**, 6645–6651.
19 B. Nie, J. G. Hu, L. B. Luo, C. Xie, L. H. Zeng, P. Lv, F. Z. Li, J. S. Jie, M. Feng, C. Y. Wu, Y. Q. Yu and S. H. Yu, *Small*, 2013, **9**, 2872–2879.
20 H. Chen, K. Liu, X. Chen, Z. Zhang, M. Fan, M. Jiang, X. Xie, H. Zhao and D. Shen, *J. Mater. Chem. C*, 2014, **2**, 9689–9694.
21 W. Dai, X. Pan, S. Chen, C. Chen, Z. Wen, H. Zhang and Z. Ye, *J. Mater. Chem. C*, 2014, **2**, 4606–4614.
22 S. Han, S. Hong, J. Ham, J. Yeo, J. Lee, B. Kang, P. Lee, J. Kwon, S. S. Lee, M. Y. Yang and S. H. Ko, *Adv. Mater.*, 2014, **26**, 5808–5814.
23 H. Guo, N. Lin, Y. Chen, Z. Wang, Q. Xie, T. Zheng, N. Gao, S. Li, J. Kang, D. Cai and D. L. Peng, *Sci. Rep.*, 2013, **3**, 2323.
24 F. Cui, Y. Yu, L. Dou, J. Sun, Q. Yang, C. Schildknecht, K. Schierle-Arndt and P. Yang, *Nano Lett.*, 2015, **15**, 7610–7615.
25 J. Chen, W. Zhou, J. Chen, Y. Fan, Z. Zhang, Z. Huang, X. Feng, B. Mi, Y. Ma and W. Huang, *Nano Res.*, 2014, **8**, 1017–1025.
26 S. Wang, Y. Cheng, R. Wang, J. Sun and L. Gao, *ACS Appl. Mater. Interfaces*, 2014, **6**, 6481–6486.
27 S. M. Jung, D. J. Preston, H. Y. Jung, Z. Deng, E. N. Wang and J. Kong, *Adv. Mater.*, 2016, **28**, 1413–1419.
28 C. Sachse, N. Weiß, N. Gaponik, L. Müller-Meskamp, A. Eychmüller and K. Leo, *Adv. Energy Mater.*, 2014, **4**, 1300737.
29 Y. Won, A. Kim, D. Lee, W. Yang, K. Woo, S. Jeong and J. Moon, *NPG Asia Mater.*, 2014, **6**, e105.
30 S. Xiao, P. Liu, W. Zhu, G. Li, D. Zhang and H. Li, *Nano Lett.*, 2015, **15**, 4853–4858.
31 W. Zhang, Z. Yin, A. Chun, J. Yoo, Y. S. Kim and Y. Piao, *ACS Appl. Mater. Interfaces*, 2016, **8**, 1733–1741.
32 Z. Chen, S. Ye, I. E. Stewart and B. J. Wiley, *ACS Nano*, 2014, **8**, 9673–9679.
33 H. Hu, L. Yu, X. Gao, Z. Lin and X. W. Lou, *Energy Environ. Sci.*, 2015, **8**, 1480–1483.
34 L. Chen, X. Li, L. Qu, C. Gao, Y. Wang, F. Teng, Z. Zhang, X. Pan and E. Xie, *J. Alloys Compd.*, 2014, **586**, 766–772.
35 M. Kevin, G. Y. R. Lim and G. W. Ho, *Green Chem.*, 2015, **17**, 1120–1126.
36 L. Xu, Y. Yang, Z. W. Hu and S. H. Yu, *ACS Nano*, 2016, **10**, 3823–3834.
37 H. J. Yang, S. Y. He and H. Y. Tuan, *Langmuir*, 2014, **30**, 602–610.
38 J. Koo, S. Kwon, N. R. Kim, K. Shin and H. M. Lee, *J. Phys. Chem. C*, 2016, **120**, 3334–3340.
39 A. Sainz-Vidal, J. Balmaseda, L. Lartundo-Rojas and E. Reguera, *Microporous Mesoporous Mater.*, 2014, **185**, 113–120.
40 E. V. Chelnokov, N. Bityurin, I. Ozerov and W. Marine, *Appl. Phys. Lett.*, 2006, **89**, 171119.